Modal Propagation Analysis with Participation Factors of Complex Frequency Variables

Dionysios Moutevelis*, Georgios Tzounas†, Javier Roldán-Pérez‡, and Federico Milano†

*Departament d'Enginyeria Electrica, CITCEA, Universitat Politécnica de Catalunya, Barcelona, Spain
† School of Electrical & Electronic Engineering, University College Dublin, Ireland
‡ Electrical Systems Unit, IMDEA Energy Institute, Madrid, Spain
dionysios.moutevelis@upc.edu, georgios.tzounas@ucd.ie, javier.roldan@imdea.org, federico.milano@ucd.ie

Abstract—This paper proposes the use of participation factors of complex frequency variables to study the propagation of oscillations in power systems. The method combines the recently proposed concept of complex frequency with modal participation analysis to derive a novel metric that locates the sources of oscillations in the system and tracks their spatial propagation. The proposed approach allows isolating the variables more sensitive to oscillations, bus voltage or frequency, thus facilitating the selection of corrective actions. The validity of the theoretical results and the scalability of the method are supported with extensive simulations performed for test networks of various sizes and with both conventional and inverter-based generation.

Index Terms—Modal propagation, power system oscillations, inverter-based resources (IBRs), small-signal stability analysis, participation factors (PFs), complex frequency (CF).

I. INTRODUCTION

A. Motivation

The wide geographic dispersion and strong coupling of frequency/voltage dynamics of Inverter-Based Resources (IBRs) makes challenging the tracking of the propagation of oscillations, the isolation of the components responsible for their initiation, and hence, also the design of efficient solutions for their mitigation. This paper proposes a computational tool and a metric for the study of frequency oscillation propagation in systems with high proliferation of IBRs. The proposed technique builds on the concept of *complex frequency*, first proposed in [1], and combines it with modal participation analysis.

B. Literature Review

A central problem for the security of low-inertia systems is understanding converter-driven frequency oscillations and the degree of their propagation in the network. In this regard, a well-known approach to study the propagation of frequency oscillations in a synchronous machine dominated system is modeling lines and generators as a distributed continuum and representing oscillations with traveling waves [2–4]. The major shortcomings of this approach are its highly topology-dependent accuracy, as well as its need for significant model simplifications. An alternative continuum model that overcomes these limitations was recently introduced based on the *frequency divider*, which provides estimations of frequency variations across a transmission network [5, 6]. Other methods focus on oscillation source localization [7–9]. These methods have been partially driven by the development and widespread use of synchronized phasor measurement units.

The starting point of the present work is an application of the concept of Complex Frequency (CF), which has been recently proposed by the last author of this paper in [1]. The CF generalizes the frequency divider and links, using minimal approximations, the different factors affecting frequency transients, complex bus power injections and their rate of change. The application of the CF has been extended to variables and signals other than voltages, including e.g. current injections and control references of power converters [10]. The CF has been also recently employed as a tool to evaluate the transient performance of IBRs [11], to estimate the inertia provided by virtual power plants [12], to draw an equivalency between complex droop and virtual oscillator controls [13], and to design a virtual impedance control for IBRs [14].

C. Contributions

This paper employs the CF concept to investigate the propagation of frequency oscillations in power networks using the generalized model analysis proposed [15].

The specific contributions of the paper are the following:

- Complex Frequency Participation Factors (CFPFs) are proposed as a novel computational tool for modal propagation analysis of power networks.
- The proposed tool is employed to study the propagation of oscillations in systems with high penetration of IBRs.

The theoretical results of this work are supported by comprehensive analysis of systems of different sizes and for various operating conditions and scenarios.

D. Paper Organization

The remainder of the paper is organized as follows. Section II recalls the definition of CF and its application to the bus voltages of a power system. Section III presents the proposed approach to study the propagation of oscillations in a power network through participation analysis of complex frequency variables. Section IV presents two case studies based on the

two-area system and the Irish transmission system, respectively. Finally, conclusions are drawn in Section V.

II. COMPLEX FREQUENCY PRELIMINARIES

In this section, we recall the mathematical definition of the CF concept, first proposed in [1], and describe its application to the bus voltages of a dynamic power system model.

A. Complex Frequency Definition

Any complex quantity, say $\bar{v}$, can be written in polar coordinates as:

$$\bar{v} = v\,e^{\jmath\,\theta}\,, \tag{1}$$

where $\jmath$ is the imaginary unit. If we define $u = \ln(v)$, $v > 0$, then (1) becomes:

$$\bar{v} = e^{u+\jmath\,\theta}\,. \tag{2}$$

If $\bar{v}$ is a function of time, then the derivative of (2) leads to:

$$\dot{\bar{v}} = (\dot{u} + \jmath\,\dot{\theta})\,e^{u+\jmath\,\theta} = (\dot{u} + \jmath\,\dot{\theta})\,\bar{v}\,. \tag{3}$$

In [1], expression (3) is applied to the bus voltages of an ac power grid written as Park vectors, namely, as time-dependent complex quantities that utilise the dq-axis components of the Park reference frame rotating at constant angular speed ω_o, i.e.:

$$\bar{v}_{\mathrm{p}} = v_d + \jmath\,v_q\,. \tag{4}$$

Differentiating (1) and (4) and taking into account the rotation of the Park reference frame, one has:

$$\omega = \dot{\theta} = \frac{v_d\dot{v}_q - v_q\dot{v}_d}{v^2} + \omega_o\,, \tag{5}$$

$$\rho = \dot{u} = \frac{\dot{v}}{v} = \frac{v_d\dot{v}_d + v_q\dot{v}_q}{v^2}\,, \tag{6}$$

where ω is the conventional instantaneous frequency of a time-varying voltage and ρ can be defined as an instantaneous bandwidth [16]. Alternatively, one can interpret ω and ρ as *azimuthal* and *radial* speeds, respectively, that describe the rotation and translation of a trajectory [17]. From (3), (5) and (6), the voltage time derivative can be written as:

$$\dot{\bar{v}} = (\rho + \jmath\,\omega)\,\bar{v} = \bar{\eta}\,\bar{v}\,, \tag{7}$$

where $\bar{\eta}$ is the *Complex Frequency (CF)* of the voltage [1].

B. Bus Voltage Complex Frequencies in a Power System

A power system model for short-term dynamic studies can be formed as a set of Differential-Algebraic Equations (DAEs):

$$\begin{aligned} \dot{\boldsymbol{x}} &= \boldsymbol{f}(\boldsymbol{x}, \boldsymbol{y})\,, \\ \boldsymbol{0}_{m,1} &= \boldsymbol{g}(\boldsymbol{x}, \boldsymbol{y})\,, \end{aligned} \tag{8}$$

where $\boldsymbol{x} = \boldsymbol{x}(t) : [0, \infty) \to \mathbb{R}^n$ and $\boldsymbol{y} = \boldsymbol{y}(t) : [0, \infty) \to \mathbb{R}^m$ are column vectors of state and algebraic variables, respectively; $\boldsymbol{f} : \mathbb{R}^{n+m} \to \mathbb{R}^n$ and $\boldsymbol{g} : \mathbb{R}^{n+m} \to \mathbb{R}^m$ are nonlinear functions; $\boldsymbol{0}_{m,1}$ is the zero matrix of dimensions $m \times 1$.

In DAEs (8) that describe the dynamic behavior of the system, bus voltages (either magnitudes and phase angles or dq-axis components) are generally represented as algebraic variables. Hence, the calculation of CFs of the bus voltages requires the definition of the voltages as functions of the states of the system i.e., $\bar{\boldsymbol{v}}(\boldsymbol{x})$. However, such expressions cannot be obtained explicitly. We deal with this problem by taking advantage of a property of the CF, i.e. it can always be obtained as the solution of a set of linear – possibly time-varying – equations, despite (8) being nonlinear. This property is demonstrated below.

Let us consider the current injections at the network buses, say $\bar{\boldsymbol{\imath}}$. These are linked to the bus voltages through the well-known admittance matrix $\bar{\boldsymbol{Y}}$:

$$\bar{\boldsymbol{\imath}} = \bar{\boldsymbol{Y}}\,\bar{\boldsymbol{v}}\,. \tag{9}$$

If the network has ν buses, then, $\bar{\boldsymbol{\imath}}$ and $\bar{\boldsymbol{v}}$ are $\nu \times 1$ vectors and $\bar{\boldsymbol{Y}}$ is a $\nu \times \nu$ matrix. Let us also assume that the elements of the voltage and current vectors are the time-dependent components of the dq-axis Park reference frame. Finally, we also assume that the elements of the admittance matrix $\bar{\boldsymbol{Y}}$ are constant, or, equivalently, that the fast dynamics of the transmission lines and transformers are negligible. Then, from (7), the time derivative of (9) is:

$$\dot{\bar{\boldsymbol{\imath}}} = \bar{\boldsymbol{Y}}\,(\bar{\boldsymbol{\eta}} \circ \bar{\boldsymbol{v}}) = \bar{\boldsymbol{Y}}\bar{\boldsymbol{V}}\,\bar{\boldsymbol{\eta}} = \bar{\boldsymbol{I}}\,\bar{\boldsymbol{\eta}}\,, \tag{10}$$

where $\circ$ indicates the Hadamard product of two vectors; $\bar{\boldsymbol{V}} = \mathrm{diag}(\bar{\boldsymbol{v}})$; and $\bar{\boldsymbol{I}} = \bar{\boldsymbol{Y}}\bar{\boldsymbol{V}}$.

The elements of the current injections $\bar{\boldsymbol{\imath}}$ are, in general, functions of state and algebraic variables. For the sake of derivation, it is convenient to separate the dq-axis components $\boldsymbol{v}_d$ and $\boldsymbol{v}_q$ of the bus voltages from other algebraic variables. Let us indicate with $\hat{\boldsymbol{y}}$ the remaining algebraic variables so that $\boldsymbol{y} = (\hat{\boldsymbol{y}}, \boldsymbol{v}_d, \boldsymbol{v}_q) := [\hat{\boldsymbol{y}}^{\mathsf{T}}, \boldsymbol{v}_d^{\mathsf{T}}, \boldsymbol{v}_q^{\mathsf{T}}]^{\mathsf{T}}$ (where T is the transpose). Since the network has ν buses, $\boldsymbol{v}_d$ and $\boldsymbol{v}_q$ are $\nu \times 1$ vectors and $\hat{\boldsymbol{y}}$ is a $(m - 2\nu) \times 1$ vector. Then, we can write:

$$\bar{\boldsymbol{\imath}} = \bar{\boldsymbol{\imath}}(\boldsymbol{x}, \hat{\boldsymbol{y}}, \boldsymbol{v}_d, \boldsymbol{v}_q)\,, \tag{11}$$

and differentiation with respect to time gives:

$$\dot{\bar{\boldsymbol{\imath}}} = \bar{\boldsymbol{\imath}}_{\boldsymbol{x}}\,\dot{\boldsymbol{x}} + \bar{\boldsymbol{\imath}}_{\hat{\boldsymbol{y}}}\,\dot{\hat{\boldsymbol{y}}} + \bar{\boldsymbol{\imath}}_{\boldsymbol{v}_d}\,\dot{\boldsymbol{v}}_d + \bar{\boldsymbol{\imath}}_{\boldsymbol{v}_q}\,\dot{\boldsymbol{v}}_q\,. \tag{12}$$

From (8), the time derivative of the full column vector of algebraic variables can be written as:[1]

$$\dot{\boldsymbol{y}} = -\boldsymbol{g}_{\boldsymbol{y}}^{-1}\boldsymbol{g}_{\boldsymbol{x}}\dot{\boldsymbol{x}} = \boldsymbol{G}\,\dot{\boldsymbol{x}}\,, \tag{13}$$

where $\boldsymbol{G}$ has dimensions $m \times n$. The submatrix $\hat{\boldsymbol{G}}$, with dimensions $(m - 2\nu) \times n$, formed with the rows of $\boldsymbol{G}$ that correspond to the subset of algebraic variables $\hat{\boldsymbol{y}}$, gives:

$$\dot{\hat{\boldsymbol{y}}} = \hat{\boldsymbol{G}}\,\dot{\boldsymbol{x}}\,. \tag{14}$$

Then, observe that the time derivatives of $\boldsymbol{v}_d$ and $\boldsymbol{v}_q$ can be written as functions of $\boldsymbol{v}_d$ and $\boldsymbol{v}_q$ as well as of the components $\boldsymbol{\rho}$ and $\boldsymbol{\omega}$ of the complex frequency, as follows:

$$\begin{aligned} \dot{\boldsymbol{v}}_d &= \boldsymbol{V}_d\,\boldsymbol{\rho} - \boldsymbol{V}_q\,\boldsymbol{\omega}\,, \\ \dot{\boldsymbol{v}}_q &= \boldsymbol{V}_q\,\boldsymbol{\rho} + \boldsymbol{V}_d\,\boldsymbol{\omega}\,, \end{aligned} \tag{15}$$

---

[1]Note that (13) requires that $\boldsymbol{g}_{\boldsymbol{y}}$ is invertible not only at an equilibrium point, but at every instant t along the flow of the solution of (8).

where $\boldsymbol{V}_d = \mathrm{diag}(\boldsymbol{v}_d)$ and $\boldsymbol{V}_q = \mathrm{diag}(\boldsymbol{v}_q)$.

Merging (10), (12), (14) and (15) and splitting real and imaginary parts, one obtains:

$$\boldsymbol{\chi} = \boldsymbol{B}\,\dot{\boldsymbol{x}}\,, \tag{16}$$

where $\boldsymbol{\chi} = (\boldsymbol{\rho},\,\boldsymbol{\omega})$, and $\boldsymbol{B}$ has dimensions $2\nu \times n$ and can be obtained as:

$$\boldsymbol{B} = \boldsymbol{H}^{-1}\boldsymbol{K}\,. \tag{17}$$

Matrix $\boldsymbol{H}$ has dimensions $2\nu \times 2\nu$ and its order is twice the number of buses of the grid. $\boldsymbol{H}$ has the following structure:

$$\boldsymbol{H} = \begin{bmatrix} \mathrm{Re}\{\bar{\boldsymbol{I}}\} & -\mathrm{Im}\{\bar{\boldsymbol{I}}\} \\ \mathrm{Im}\{\bar{\boldsymbol{I}}\} & \mathrm{Re}\{\bar{\boldsymbol{I}}\} \end{bmatrix} - \begin{bmatrix} \mathrm{Re}\{\bar{\boldsymbol{I}}_1\} & \mathrm{Re}\{\bar{\boldsymbol{I}}_2\} \\ \mathrm{Im}\{\bar{\boldsymbol{I}}_1\} & \mathrm{Im}\{\bar{\boldsymbol{I}}_2\} \end{bmatrix}, \tag{18}$$

with

$$\bar{\boldsymbol{I}}_1 = \bar{\boldsymbol{i}}_{\boldsymbol{v}_d}\boldsymbol{V}_d + \bar{\boldsymbol{i}}_{\boldsymbol{v}_q}\boldsymbol{V}_q\,,$$
$$\bar{\boldsymbol{I}}_2 = \bar{\boldsymbol{i}}_{\boldsymbol{v}_q}\boldsymbol{V}_d - \bar{\boldsymbol{i}}_{\boldsymbol{v}_d}\boldsymbol{V}_q\,.$$

Finally, the $2\nu \times n$ matrix $\boldsymbol{K}$ is:

$$\boldsymbol{K} = \begin{bmatrix} \mathrm{Re}\{\bar{\boldsymbol{i}}_{\boldsymbol{x}}\} + \mathrm{Re}\{\bar{\boldsymbol{i}}_{\boldsymbol{y}}\}\hat{\boldsymbol{G}} \\ \mathrm{Im}\{\bar{\boldsymbol{i}}_{\boldsymbol{x}}\} + \mathrm{Im}\{\bar{\boldsymbol{i}}_{\boldsymbol{y}}\}\hat{\boldsymbol{G}} \end{bmatrix}. \tag{19}$$

III. COMPLEX FREQUENCY PARTICIPATION FACTORS

In this section, we first recall standard small-signal stability analysis using modal participation factors in the classical sense. We then present the proposed approach to study the propagation of dynamic modes in power networks through participation factor analysis of complex frequency variables.

A. Classical Small-Signal Stability Analysis

Consider that an equilibrium $(\boldsymbol{x}_o, \boldsymbol{y}_o)$ of (8) is known. Then, small-disturbance analysis permits linearization of (8) around the equilibrium, as follows:

$$\dot{\tilde{\boldsymbol{x}}} = \boldsymbol{f}_{\boldsymbol{x}}\tilde{\boldsymbol{x}} + \boldsymbol{f}_{\boldsymbol{y}}\tilde{\boldsymbol{y}}\,, \tag{20}$$
$$\boldsymbol{0}_{m,1} = \boldsymbol{g}_{\boldsymbol{x}}\tilde{\boldsymbol{x}} + \boldsymbol{g}_{\boldsymbol{y}}\tilde{\boldsymbol{y}}\,, \tag{21}$$

where $\tilde{\boldsymbol{x}} = \boldsymbol{x} - \boldsymbol{x}_o$, $\tilde{\boldsymbol{y}} = \boldsymbol{y} - \boldsymbol{y}_o$; and $\boldsymbol{f}_{\boldsymbol{x}}$, $\boldsymbol{f}_{\boldsymbol{y}}$, $\boldsymbol{g}_{\boldsymbol{x}}$, $\boldsymbol{g}_{\boldsymbol{y}}$ are Jacobian matrices at $(\boldsymbol{x}_o, \boldsymbol{y}_o)$. From (21) and assuming that $\boldsymbol{g}_{\boldsymbol{y}}$ is full rank, we get that:

$$\tilde{\boldsymbol{y}} = -\boldsymbol{g}_{\boldsymbol{y}}^{-1}\boldsymbol{g}_{\boldsymbol{x}}\tilde{\boldsymbol{x}}\,, \tag{22}$$

and by substituting (22) in (20), we arrive to the following set of linear ordinary differential equations:

$$\dot{\tilde{\boldsymbol{x}}} = \boldsymbol{A}\,\tilde{\boldsymbol{x}}\,, \tag{23}$$

where $\boldsymbol{A} = \boldsymbol{f}_{\boldsymbol{x}} - \boldsymbol{f}_{\boldsymbol{y}}\boldsymbol{g}_{\boldsymbol{y}}^{-1}\boldsymbol{g}_{\boldsymbol{x}}$. The general solution of (23) is:

$$\tilde{\boldsymbol{x}}(t) = \boldsymbol{U}\,e^{\boldsymbol{J}t}\,\boldsymbol{W}\tilde{\boldsymbol{x}}(0)\,, \tag{24}$$

where $\boldsymbol{U}$ is modal matrix with columns n right eigenvectors; $\boldsymbol{W}$ is modal matrix with rows n left eigenvectors, i.e. $\boldsymbol{U} = \begin{bmatrix} \boldsymbol{u}_1 & \boldsymbol{u}_2 & \dots & \boldsymbol{u}_n \end{bmatrix}$, $\boldsymbol{W} = \begin{bmatrix} \boldsymbol{w}_1^{\mathsf{T}} & \boldsymbol{w}_2^{\mathsf{T}} & \dots & \boldsymbol{w}_n^{\mathsf{T}} \end{bmatrix}^{\mathsf{T}}$; eigenvectors are normalized so that $\boldsymbol{w}_i\boldsymbol{u}_i = 1$; $\boldsymbol{J}$ is the system's Jordan matrix defined as $\boldsymbol{J} = \boldsymbol{W}\boldsymbol{A}\boldsymbol{U}$ and $e^{\boldsymbol{J}t}$ its matrix exponential. Then, system (23) is asymptotically stable if for $t \to \infty$, $\tilde{\boldsymbol{x}}(t) \to \boldsymbol{0}_{n,1}$. This is true if and only if all

diagonal elements of $\boldsymbol{J}$ (i.e. the eigenvalues of the state matrix $\boldsymbol{A}$) have negative real parts.

Under the assumption that all eigenvalues λ_i, $i = 1, 2, \dots, n$ of $\boldsymbol{A}$ have equal algebraic and geometric multiplicities[2], $\boldsymbol{J}$ is diagonal and the evolution of the k-th element of $\tilde{\boldsymbol{x}}$ is:

$$\tilde{x}_k(t) = \sum_{i=1}^{n} e^{\lambda_i t}\,\boldsymbol{w}_i\,\tilde{\boldsymbol{x}}(0)\,u_{ki}\,, \tag{25}$$

where with u_{ki}, w_{ik} we denote the k-th elements of $\boldsymbol{u}_i$, $\boldsymbol{w}_i$, respectively. Moreover, by exciting in the k-th differential equation the k-th state, e.g. by applying the initial conditions $\tilde{x}_k(0) = 1$, and $\tilde{x}_h(0) = 0$, $h \neq k$ [19], we get:

$$\tilde{x}_k(t) = \sum_{i=1}^{n} w_{ik}\,u_{ki}\,e^{\lambda_i t} = \sum_{i=1}^{n} p_{ki}^{[x]}\,e^{\lambda_i t}\,, \tag{26}$$

where:

$$p_{ki}^{[x]} = w_{ik}\,u_{ki}\,, \tag{27}$$

is known as *mode-in-state participation factor* and is a classical measure of the relative contribution of the i-th dynamic mode (as represented by the eigenvalue λ_i) in the evolution of the k-th state variation $\tilde{x}_k(t)$. Then, the matrix

$$\mathbf{P}_x = (p_{ki}^{[x]})_{1 \leq (k,i) \leq n}\,, \tag{28}$$

is the system's *mode-in-state participation matrix*.

B. Proposed Complex Frequency Participation Factors

Consider a set of μ defined state-space system outputs. The k-th output $z_k \in \mathbb{R}$, $1 \leq k \leq \mu$, is defined as a nonlinear function of the system's states, as follows:

$$z_k = h(\boldsymbol{x}, \boldsymbol{y})\,, \quad 1 \leq k \leq \mu\,,$$

where $h : \mathbb{R}^n \to \mathbb{R}$. Differentiation around $(\boldsymbol{x}_o, \boldsymbol{y}_o)$ gives:

$$\tilde{z}_k = h_{\boldsymbol{x}}\tilde{\boldsymbol{x}} + h_{\boldsymbol{y}}\tilde{\boldsymbol{y}}\,, \quad 1 \leq k \leq \mu\,, \tag{29}$$

where $h_{\boldsymbol{x}}$, $h_{\boldsymbol{y}}$ are the gradients with respect to state and algebraic variables, respectively. Using (22) in (29) yields:

$$\tilde{z}_k = \boldsymbol{c}_k\,\tilde{\boldsymbol{x}} = c_{k1}\tilde{x_1} + c_{k2}\tilde{x_2} + \dots + c_{kn}\tilde{x_n}\,, \tag{30}$$

where $\boldsymbol{c}_k = h_{\boldsymbol{x}} - h_{\boldsymbol{y}}\boldsymbol{g}_{\boldsymbol{y}}^{-1}\boldsymbol{g}_{\boldsymbol{x}}$, $\boldsymbol{c}_k \in \mathbb{R}^{1 \times n}$. Equivalently:

$$\tilde{z}_k = c_{k1}\sum_{i=1}^{n} p_{1i}^{[x]}e^{\lambda_i t} + c_{k2}\sum_{i=1}^{n} p_{2i}^{[x]}e^{\lambda_i t} + \dots + c_{kn}\sum_{i=1}^{n} p_{ni}^{[x]}e^{\lambda_i t}$$

or:

$$\tilde{z}_k = \sum_{i=1}^{n}(c_{k1}p_{1i}^{[x]} + c_{k2}p_{2i}^{[x]} + \dots + c_{kn}p_{ni}^{[x]})e^{\lambda_i t} = \sum_{i=1}^{n}p_{ki}^{[z]}e^{\lambda_i t}$$

where we define

$$p_{ki}^{[z]} = c_{k1}p_{1i}^{[x]} + c_{k2}p_{2i}^{[x]} + \dots + c_{kn}p_{ni}^{[x]}\,, \tag{31}$$

[2]Note that this comes with simplicity but with no loss of generality. For the general case of a dynamical system that includes eigenvalues whose geometric multiplicity $\neq$ algebraic multiplicity, the interested reader is referred to [18].

as the *mode-in-output participation factor*. The quantity $p_{ki}^{[z]}$ determines the relative contribution of the i-th dynamic system mode in the evolution of the l-th system output $\tilde{z}_l(t)$. To ensure that the participation factors that correspond to different outputs are comparable independently of their units and gains, (31) is normalized, as follows:

$$p_{ki}^{[z]} = \frac{c_{k1}\, p_{1i}^{[x]} + c_{k2}\, p_{2i}^{[x]} + \ldots + c_{kn}\, p_{ni}^{[x]}}{||\boldsymbol{c}_k||}, \quad (32)$$

where $||\cdot||$ denotes the Euclidean norm.

Assembling all μ system output rows in a single matrix $\boldsymbol{C} = \begin{bmatrix} \boldsymbol{c}_1^{\mathsf{T}} & \boldsymbol{c}_2^{\mathsf{T}} & \ldots & \boldsymbol{c}_\mu^{\mathsf{T}} \end{bmatrix}^{\mathsf{T}}$, the participation matrix $\mathbf{P}_z$ corresponding to the output column vector:

$$\tilde{\boldsymbol{z}} = \boldsymbol{C}\,\tilde{\boldsymbol{x}}, \quad (33)$$

is

$$\mathbf{P}_z = \boldsymbol{C}\,\mathbf{P}_x, \quad (34)$$

where $\mathbf{P}_z = (p_{ki}^{[z]})_{1 \leq k \leq \mu, 1 \leq i \leq n}$, is called the system's *mode-in-output participation matrix*.

An important special case for the ouput matrix is $\boldsymbol{C} = -\boldsymbol{g_y}^{-1}\boldsymbol{g_x}$, for which $\mathbf{P}_z$ corresponds to the participation matrix $\mathbf{P}_y$ of the system's algebraic variables [15]:

$$\mathbf{P}_y = -\boldsymbol{g_y}^{-1}\boldsymbol{g_x}\,\mathbf{P}_x. \quad (35)$$

We proceed to define the proposed participation factors of complex frequency variables. To this aim, we note that equation (16) is valid at any point of a transient, including equilibria. At an equilibrium, merging (23) and (16) gives:

$$\tilde{\boldsymbol{\chi}} = \boldsymbol{B}\,\boldsymbol{A}\,\tilde{\boldsymbol{x}}, \quad (36)$$

which is in the same form as (33), with $\boldsymbol{C} = \boldsymbol{B}\,\boldsymbol{A}$. Thus, following from (33), (34), and (36), we propose computing the $2\nu \times n$ participation factors that link the real ($\boldsymbol{\rho}$) and imaginary ($\boldsymbol{\omega}$) parts of the bus CFs to the oscillatory modes of the system, as follows:

$$\mathbf{P}_\chi = \boldsymbol{B}\,\boldsymbol{A}\,\mathbf{P}_x. \quad (37)$$

It is also relevant to define the participation factors of $\boldsymbol{\eta}$, which provide information regarding the combined impact of oscillatory modes on the rate of change of both voltage magnitudes and phase angles. We propose the following definition of these participation factors. Let $\boldsymbol{B}_\rho$ and $\boldsymbol{B}_\omega$ be the matrices composed of the first and last ν rows, respectively, of $\boldsymbol{B}$. Then, we define the complex $\nu \times n$ participation matrix $\bar{\mathbf{P}}_\eta$ as:

$$\bar{\mathbf{P}}_\eta = (\boldsymbol{B}_\rho + \jmath\boldsymbol{B}_\omega)\,\boldsymbol{A}\,\mathbf{P}_x, \quad (38)$$

and the real $\nu \times n$ participation matrix $\mathbf{P}_\eta$ as the matrix composed of the absolute values of the elements of $\bar{\mathbf{P}}_\eta$, which, with a loose notation, one can write as:

$$\mathbf{P}_\eta = |\bar{\mathbf{P}}_\eta|. \quad (39)$$

The elements of $\mathbf{P}_\chi$ and $\mathbf{P}_\eta$ are the CFPFs that we use in the remainder of this work as a computational tool to study the propagation of oscillations across power system networks.

IV. CASE STUDIES

This section presents two case studies. The first is based on the well-known two-area benchmark system [20] and illustrates how CFPFs capture the spatial distribution of oscillations under different scenarios. The second case study considers a detailed model of the all-island Irish transmission system and demonstrates the ability of the proposed technique to track the propagation of both critical, low-frequency and non-critical, high frequency modes in a large, realistic model of a power system.

All results in this section are produced with the software tool Dome [21], wherein standard linear algebra calculations are performed with LAPACK [22]. CFPFs are calculated with the procedure described in Section II.

A. Two-area System

The single-line diagram of the system is shown in Fig. 1. It comprises two areas connected to each other with a double tie-line; 11 buses and 4 Synchronous Generators (SGs), G1-G4. Each SG is modelled with a 6-th order model and equipped with an Automatic Voltage Regulator (AVR) and a Turbine Governor (TG) [20]. The system feeds the loads connected to buses 7 and 9.
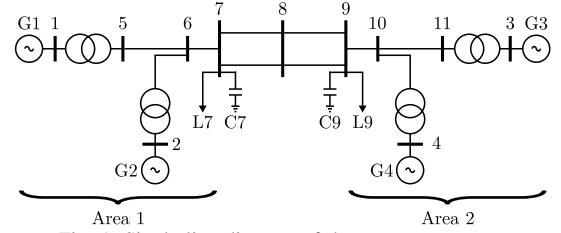

Fig. 1: Single-line diagram of the two-area system.

1) Validation for Interarea Electromechanical Oscillations: In this section, we illustrate the information provided by the proposed CFPFs on the original two-area system. To this aim, we start by carrying out an eigenvalue analysis, which indicates that the system is stable, and that the most critical complex pair of eigenvalues is $-0.071 \pm 3.429\jmath$, with natural frequency 0.55 Hz and damping ratio 2.08 %. This pair represents the system's interarea electromechanical mode between Areas 1 and 2.

Classical Participation Factor (PF) analysis provides information on the most dominant for the interarea mode state variables, yet it does not reveal how the mode propagates across the network's buses. In this case, the most dominant variables are the rotor angles and speeds of generators G3 and G4, followed by a relatively smaller contribution of the angles and speeds of generators G1 and G2. The PFs of the SG rotor speeds for the interarea mode are summarized in Table I (original system).

The information of how the system's modes propagate along the network can be acquired through the proposed CFPFs. With this goal, we proceed to compute matrix $\bar{\mathbf{P}}_\eta$ from (39). The results for the interarea mode are presented in Fig. 2a in the form of a graph, where the size and color of each vertex

TABLE I: Two-area system: PFs of interarea mode in SG speeds. Results are given for the original system and for the modified system with halved distance between Areas 1 and 2.

ω	PF (original system)	PF (modified system)
G1	0.0256	0.1580
G2	0.0135	0.0517
G3	0.2729	0.2100
G4	0.1496	0.0846

(a) Original system.

(b) Modified system with halved distance between Areas 1 and 2.
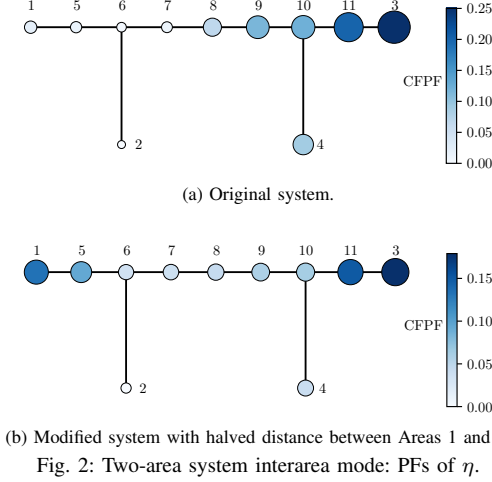
Fig. 2: Two-area system interarea mode: PFs of η.

is setup according to the magnitude of the corresponding bus CFPF, illustrating the tracking of the mode at any network bus by the proposed method. Moreover, a check of the values of CFPFs at the buses where G1-G4 are connected confirms that the results are consistent with those of the classical analysis of Table I. The graphs in Fig. 2a have been generated with the Python library *networkx* [23].

We further check the ability of CFPFs to track the propagation of interarea oscillations along the network. To this aim, the original two-area system is modified by reducing by 50 % the length of the double line that interconnects Areas 1 and 2. Eigenvalue analysis of the modified system shows that the interarea mode is now given by the complex pair $-0.141 \pm 5.002 \jmath$. Moreover, classical PF analysis (see Table I) indicates that, compared to the original system, the contribution to interarea oscillations of SGs from Area 1 (i.e. G1 and G2), has significantly increased, whereas the contribution of generators from Area 2 (i.e. G3 and G4), has relatively decreased. Again, the change on the propagation of the mode at each bus of the network due to the system modification can not be tracked by classical PF analysis. To do that, we calculate the bus CFPFs. The CFPF results are illustrated in Fig. 2b. Viewing these results in comparison to Table I further confirms the alignment of the proposed approach with classical PF analysis at generator buses.

2) Grid-Forming (GFM) Converter-Driven Oscillations: In this section, we showcase the ability of CFPFs to capture the propagation of high-frequency oscillations driven by converter-interfaced generators. With this goal, the conventional generator G1 is replaced by a Virtual Synchronous Machine (VSM) of same rating. The VSM synchronization loop is modelled as

in [24], while the inner current and voltage control loops are modelled as in [25]. The power injected by the converter to the network is provided by an ideal voltage source connected to the dc-side of the converter.

For the purposes of this scenario, we include in the system unsuppressed oscillations by setting the damping parameter in the VSM loop to zero. Figure 3 shows, through the CFPFs of ρ, ω and η, how three selected dynamic modes propagate across the network buses. These include two critical modes, namely Mode 1 and Mode 2, with corresponding eigenvalues $-0.73 \pm 41.76 \jmath$ and $-0.16 \pm 3.92 \jmath$, and damping ratios 1.74 % and 4.02 %, respectively, as well as a high-frequency mode, namely Mode 3, with eigenvalues $(-0.25 \pm 1.2 \jmath) \cdot 10^6$ and damping ratio 20.85 %.

CFPFs indicate bus 1, i.e. the VSM connection bus, as the source of the oscillatory Mode 1, with CFPF values remaining high for buses located close to the connection point (Area 1). Given the higher values of ρ PFs over ω PFs, it is deduced that bus voltage magnitudes are more susceptible to Mode 1 than phase angles. This information is of particular interest for cases where the complex VSM control structure deteriorates the frequency/voltage decoupling of the grid [26].
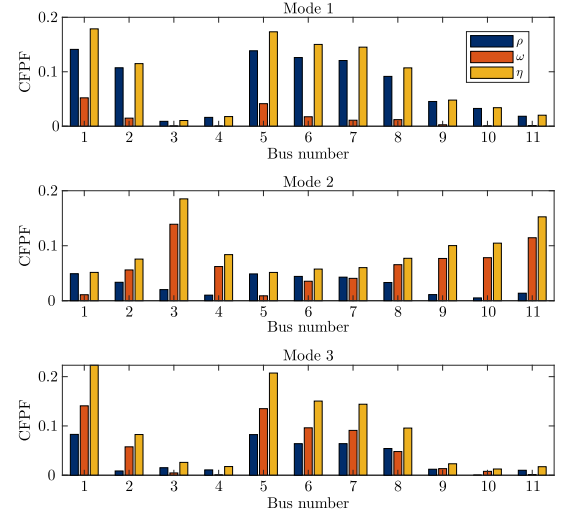

Fig. 3: Modified two-area system with GFM converter at bus 1: CFPFs of Modes 1-3.

CFPFs also indicate that G3 is the source of Mode 2. Moreover, apart from locating the oscillation source, CFPF analysis also provides insights on the physical interpretation of the oscillation. Namely, the higher values for the PFs of ω compared to the ones of ρ, tie the oscillation to the phase angles of the voltages at the connection bus, which are in turn linked to the rotor angle/speed of the generators.

Similarly to Mode 1, the CFPFs for Mode 3 indicate that the VSM connection bus has the highest participation to this mode. Compared to Mode 1, however, it can be seen that the participation of network buses decreases radically along the long transmission lines that interconnect Areas 1 and 2. This observation aligns with the current understanding that high frequency modes do not effectively propagate through long inductive lines. The above analysis of Modes 1-3 also
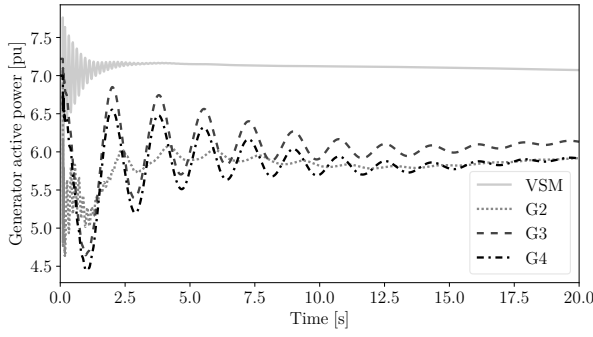
Fig. 4: Modified two-area system with GFM converter at bus 1: Active power injections of VSM, G2, G3 and G4 after the disconnection of 38 % of the load at bus 7.
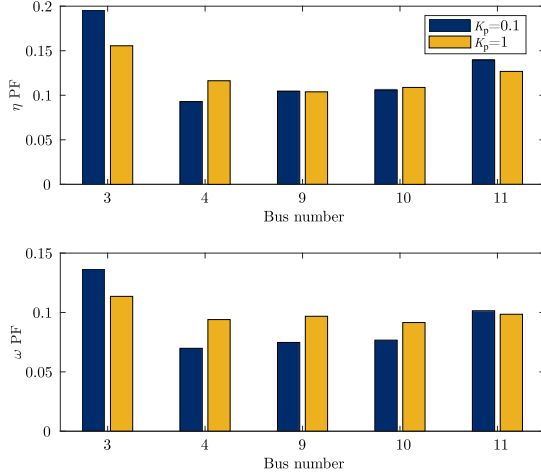

Fig. 5: Modified two-area system with GFL load at bus 9: CFPFs of critical mode for Area 2. Two different values for gain K_p of the outer loops of the GFL converter are used.
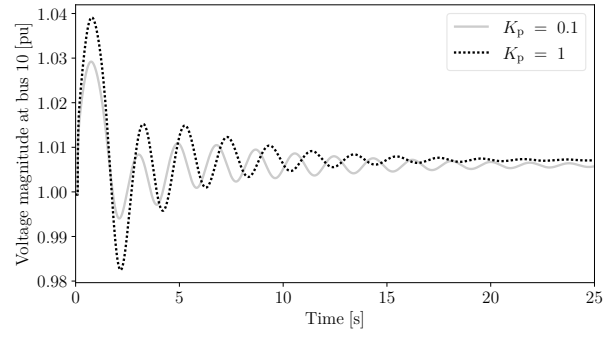

Fig. 6: Modified two-area system with GFL load at bus 9: Voltage magnitude at bus 10 after disconnecting 6.92 % of the load at bus 7. Different values for gain K_p of the outer control loop of the GFL converter, connected at bus 9, are used.

channel is used for ac voltage support. The proportional gain K_p of the outer PI controllers is set initially to 0.1 for both channels and it is increased subsequently to $K_\mathrm{p} = 1$.

Figure 5 shows the PFs for η and ω and for the buses of Area 2 of the system. For the first parameter setting ($K_\mathrm{p} = 0.1$) a critical mode exists with corresponding eigenvalues $-0.1187 \pm 3.2792\jmath$ and damping 3.62 %. For the second parameter setting ($K_\mathrm{p} = 1$), the eigenvalues corresponding to the same mode become $-0.1924 \pm 3.0162\jmath$ and the damping increases to 6.37 %. The distribution of the PFs of η identifies G3 as the source participating mostly in the mode, for both parameter settings. The distribution of ω PFs provides additional information. Firstly, it can be seen that their values remain high across a wider portion of buses and with no gradual decrease, moving away from the generator. Also, variable ω_9 of bus 9 contributes more to the critical mode, despite being connected to a different bus than G3 and G4. This indicates that a device contributing to the increased damping of the mode is connected to that specific bus. This example demonstrates that the trend shown for the previous cases, i.e. the CFPFs being larger at the connection point of the sources and decreasing moving away from them, can be reversed in the presence of converter-interfaced, non-synchronous devices. The proposed method tracks the oscillation propagation in the network and implicitly considers the change in the parameter setup and its effect on the system damping.

Finally, to showcase the increased damping by the GFL converter, a time-domain simulation is performed. The contingency applied is the loss of 6.92 % of the load at bus 7 at $t = 0.1$ s. Figure 6 shows the voltage response at bus 10 after the contingency, and for the two different control parameter values, i.e. $K_\mathrm{p} = \{0.1, 1\}$. It is verified that, despite the increased overshoot, the post-contingency oscillations are damped more quickly for $K_\mathrm{p} = 1$.

B. Irish Transmission System

For this case, a model of the all-island, Irish power system is used [27]. The system used for this study consists of 1479 buses, 1851 transmission lines and transformers, 22 conventional SGs, along with their appropriate control systems, 169 wind power plants and 245 loads. This application showcases
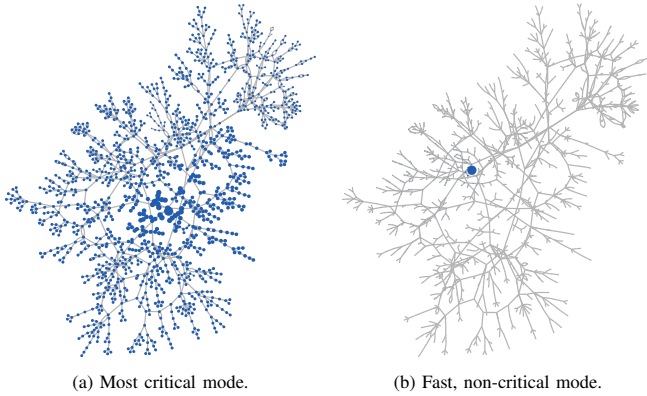
shows that CFPFs are able to capture the evolution through the network of oscillations of different nature and timescales, which can be present concurrently in the same system.

Figure 4 shows the active power injections of VSM, G2, G3 and G4, after the disconnection of 38 % of the load at bus 7 at $t = 0.1$ s. The time response is consistent with the findings of CFPF analysis, illustrating the timescale difference between the two undamped modes (Mode 1 and 2), and confirming that devices connected to dominant buses are indeed strongly linked to these modes. Additionally, it highlights how the calculation of the PFs of ρ and ω offers complementary information, not easily discernible from time domain simulations, on the type of buses' susceptance to these oscillations.

3) Damping from Grid-Following (GFL) Loads: This section showcases an application of the CFPF analysis when the control systems of non-synchronous devices affect the system's damping. For this scenario, the original two-area system is modified to substitute the static load at bus 9 with a converter-interfaced load of the same steady-state power consumption. All four conventional SGs remain connected. For the converter, a standard GFL, cascaded control configuration is used, as in [10, 25]. The d-channel of the outer control loop is regulating the active power load consumption while the q-

(a) Most critical mode.   (b) Fast, non-critical mode.

Fig. 7: Irish system: CFPFs of η.

the scalability of the proposed method as well as the effect that the timescale of a mode has on its ability to propagate in a large network.

For the illustration of modal propagation, two modes are selected. Their representing eigenvalues are $-0.003 \pm 2.43\jmath$ and $-1.9 \pm 10.95\jmath$, with natural frequencies 0.387 Hz and 1.743 Hz and damping ratios 0.11 % and 17.17 %, respectively. One should note that from the selected modes, the first one is critical while the second one is non-critical. These modes are obtained by adapting the parameter tuning of the Irish system for illustration purposes and do not represent the actual dynamics of the system. Figures 7a-7b show the distribution of the CFPFs of η in the form of network graphs, with the size of each vertex depending on the CFPF value. The Irish network graphs are generated using the Python module *graph-tool* [28]. We note that the position of each vertex in the graph does not represent the actual geography of the Irish network.

Figure 7a shows the participation of the different network buses for the slow mode ($-0.003 \pm 2.43\jmath$). It can be seen that the oscillation is visible in most of the network buses. In comparison, Figure 7b shows the participation of the buses to the high frequency mode ($-1.9 \pm 10.95\jmath$). It can be seen that only the connection bus of the oscillation source presents a high PF value while the participation of the rest of the system buses sharply diminishes.

V. CONCLUSIONS

The paper proposes the use of participation factors of CF variables as a metric for the analysis of modal propagation in power systems. The theoretical appraisal and simulation results show that the proposed approach has several relevant features. First, it identifies the source of potential oscillations in the system and is able to capture the modal propagation through the grid, thus providing an indication on the areas that are more affected by such oscillations. Simulation results based on the Irish transmission system also indicate that low-frequency modes can propagate across a large part of the network while damped, faster modes are generally contained in a small part of the network. Then, the PFs of the real and imaginary part of the CF provide information on the oscillation type, i.e. whether it affects more the voltage or the frequency. This

gives a better understanding of the problem and facilitates the selection of appropriate corrective measures. For example, in the case of IBRs, it provides information on dynamic coupling among converter controllers and facilitates the tuning of the converter control parameters. The control-design capabilities of the proposed technique will be the focus of future work.

REFERENCES

[1] F. Milano, "Complex frequency," *IEEE Trans. on Power Systems*, vol. 37, no. 2, pp. 1230–1240, 2022.

[2] A. Semlyen, "Analysis of disturbance propagation in power systems based on a homogeneoue dynamic model," *IEEE Trans. on Power Apparatus and Systems*, no. 2, pp. 676–684, 1974.

[3] J. S. Thorp, C. E. Seyler, and A. G. Phadke, "Electromechanical wave propagation in large electric power systems," *IEEE Trans. on Circuits and Systems I: Fundamental Theory and Applications*, vol. 45, no. 6, pp. 614–622, 1998.

[4] D. Huang, J. Qin, H. Liu, J. H. Chow, J. Zhao, T. Bi, L. Mili, and Q. Yang, "An analytical method for disturbance propagation investigation based on the electromechanical wave approach," *IEEE Trans. on Power Systems*, vol. 36, no. 2, pp. 991–1001, 2020.

[5] F. Milano and Á. Ortega, "Frequency divider," *IEEE Trans. on Power Systems*, vol. 32, no. 2, pp. 1493–1501, 2016.

[6] G. Tzounas, I. Dassios, and F. Milano, "Frequency divider as a continuum," *IEEE Trans. on Power Systems*, vol. 37, no. 6, pp. 4970–4973, 2022.

[7] J.-A. Jiang, J.-Z. Yang, Y.-H. Lin, C.-W. Liu, and J.-C. Ma, "An adaptive PMU based fault detection/location technique for transmission lines. I. Theory and algorithms," *IEEE Trans. on Power Delivery*, vol. 15, no. 2, pp. 486–493, 2000.

[8] J. Ma, P. Zhang, H.-j. Fu, B. Bo, and Z.-y. Dong, "Application of phasor measurement unit on locating disturbance source for low-frequency oscillation," *IEEE Trans. on smart grid*, vol. 1, no. 3, pp. 340–346, 2010.

[9] L. Chen, Y. Min, and W. Hu, "An energy-based method for location of power system oscillation source," *IEEE Trans. on Power Systems*, vol. 28, no. 2, pp. 828–836, 2012.

[10] D. Moutevelis, J. Roldán-Pérez, M. Prodanovic, and F. Milano, "Taxonomy of power converter control schemes based on the complex frequency concept," *IEEE Trans. on Power Systems*, 2023.

[11] W. Zhong, G. Tzounas, and F. Milano, "Improving the power system dynamic response through a combined voltage-frequency control of distributed energy resources," *IEEE Trans. on Power Systems*, vol. 37, no. 6, pp. 4375–4384, 2022.

[12] W. Zhong, G. Tzounas, M. Liu, and F. Milano, "On-line inertia estimation of virtual power plants," *Elec. Power Sys. Research*, vol. 212, p. 108336, 2022.

[13] X. He, V. Häberle, I. Subotić, and F. Dörfler, "Nonlinear stability of complex droop control in converter-based power systems," *IEEE Control Systems Letters*, vol. 7, pp. 1327–1332, 2023.

[14] D. Moutevelis, J. Roldán-Pérez, M. Prodanovic, and F. Milano, "Design of virtual impedance control loop using the complex frequency approach," in *2023 IEEE Belgrade PowerTech*. IEEE, 2023, pp. 1–6.

[15] G. Tzounas, I. Dassios, and F. Milano, "Modal participation factors of algebraic variables," *IEEE Trans. on Power Systems*, vol. 35, no. 1, pp. 742–750, 2019.

[16] L. Cohen, *Time-Frequency Analysis: Theory and Applications*. Upper Saddle River, NJ: Prentice-Hall Signal Processing, 1995.

[17] F. Milano, G. Tzounas, I. Dassios, and T. Kërçi, "Applications of the Frenet frame to electric circuits," *IEEE Trans. on Circuits and Systems I: Regular Papers*, vol. 69, no. 4, pp. 1668–1680, 2022.

[18] I. Dassios, G. Tzounas, and F. Milano, "Participation factors for singular systems of differential equations," *Circuits, Systems, and Signal Processing*, vol. 39, pp. 83–110, 2020.

[19] I. J. Pérez-Arriaga, G. C. Verghese, and F. C. Schweppe, "Selective modal analysis with applications to electric power systems, Part I: Heuristic introduction," *IEEE Trans. on Power Apparatus and Systems*, vol. PAS-101, no. 9, pp. 3117–3125, Sep. 1982.

[20] P. S. Kundur and O. P. Malik, *Power system stability and control.* McGraw-Hill Education, 2022.

[21] F. Milano, "A Python-based software tool for power system analysis," in *IEEE PES General Meeting*. IEEE, 2013, pp. 1–5.

[22] E. Anderson, Z. Bai, C. Bischof, J. Demmel, J. Dongarra, J. DuCroz, A. Greenbaum, S. Hammarling, A. McKenney, and D. Sorensen, "LA-PACK: A portable linear algebra library for high-performance computers," 1990.

[23] A. Hagberg, P. Swart, and D. S Chult, "Exploring network structure, dynamics, and function using networkx," Los Alamos National Lab.(LANL), Los Alamos, NM (United States), Tech. Rep., 2008.

[24] A. González-Cajigas, J. Roldán-Pérez, and E. J. Bueno, "Design and analysis of parallel-connected grid-forming virtual synchronous machines for island and grid-connected applications," *IEEE Trans. on Power Electronics*, vol. 37, no. 5, pp. 5107–5121, 2021.

[25] Á. Ortega and F. Milano, "Generalized model of VSC-based energy storage systems for transient stability analysis," *IEEE Trans. on Power Systems*, vol. 31, no. 5, pp. 3369–3380, 2015.

[26] J. Roldán-Pérez, A. Rodríguez-Cabero, and M. Prodanovic, "Design and analysis of virtual synchronous machines in inductive and resistive weak grids," *IEEE Trans. on En. Conv.*, vol. 34, no. 4, pp. 1818–1828, 2019.

[27] G. M. Jónsdóttir and F. Milano, "Stochastic modeling of tidal generation for transient stability analysis: A case study based on the all-island Irish transmission system," *Electric Power Systems Research*, vol. 189, p. 106673, 2020.

[28] T. P. Peixoto, "The graph-tool Python library," *figshare*, 2014, available at graph-tool.skewed.de.